PHASE TRANSFORMATIONS ON STEEL DURING INDUCTION HARDENING

D. Gaude-Fugarolas (Cambridge University, United Kingdom, Cambridge)

ABSTRACT

Steel components for many critical applications need to be produced to meet very high standards of dimensional accuracy, mechanical properties and microstructure. One example of that are components for the automotive industry, which at the same time have to be produced in large quantities and in highly reliable processes. Some of the advantages of induction hardening are that it allows to automate the heat-treating of large batches of components, of many symmetries and sizes, producing a localised hardened layer and very small distortion. A comprehensive model to determine the microstructure evolution during induction hardening of hypoeutectoid steel components has been developed. The model includes the calculation of the thermal history during the process and takes into account the composition and microstructure, as well as several process parameters.

Introduction:

Induction hardening has become very popular in automated manufacturing processes in which large series of axisymmetric or near-axisymmetric steel or cast-iron components have to be heat-treated. An alternating magnetic field is applied to the metallic component, and by induction, eddie currents are generated at the surface of the component. Such currents heat the metal by Joule effect to the desired temperature and the component can then be spray or immersion quenched. Induction produces a very fast and reliable heating, and it is a method suited for all sizes of components. It is also suitable for localised heat treatment and to obtain different depths of hardened case (Ref.1).

Understanding and being able to predict the microstructure evolution during induction hardening is of vital importance when monitoring and optimising such manufacturing process. For that purpose, a model on austenitisation of hypoeutectoid steel and subsequent quenching has been developed (Ref.2). It has been decided that a completely modular approach was more flexible. The induction hardening model presented in this work is composed of three independent submodels. The temperature cycle at each point whithin the part studied is determined first, from the geometry of the part, the thermal properties of the alloy and the characteristics of the process. The temperature evolution curves thus obtained are fed into the austenitisation submodel to determine the extent of the transformation to austenite, as a function of position in the part, during the induction heating stage of the process. Finally, the decomposition of such austenite can be modelled using the quench submodel and the temperature evolution curves for quenching determined previously.

Determination of the heat cycle:

To determine the temperature evolution during induction hardening the heat transfer differential equation [1] has been integrated using the Crank-Nicholson method (Ref.3). Two part geometries are considered, a plate and a cylinder. Temperature and position are normalised and represented by u and x (plate) or r (cylinder), defined as 0 at the center of the plate/cylinder and 1 at its surface.

The initial condition is [2] and the boundary conditions are [3] for simmetry and [4] during heating and [5] during cooling.

Heating is assumed to occur by the introduction of a constant flux of heat at the surface of the part, until it reaches a target temperature. The induction phase of the process ends and after a short dead time, during which only air convection cools the component, the water spraying system starts to operate and quenches the component to room temperature.

An example of the curves obtained for a thick plate is shown in Fig.1.

Austenitisation:

The phenomena associated with the austenitisation of a hypoeutectoid steel are more complex than for the same transformation in other alloys. The equilibrium microstructure is composed of allotriomorphic ferrite and pearlite, the latter being a composite of ferrite and cementite. In two-dimensional sections a colony of pearlite has the appearance of alternate lamellae of ferrite and cementite. In three dimensions, each colony consists of an interpenetrating bi-crystal of ferrite and cementite. Ferrite has a very low solubility for carbon and hence, on its own, only begins to transform to austenite at high temperatures. But if cementite decomposes and yields its carbon to the transformation front, the reaction from ferrite to austenite can proceed at lower temperatures.

It is logical to expect that the initiation of austenitisation in a hypoeutectoid steel is in pearlite, where the diffusion distances for carbon are small. The reaction can then proceed into the remaining ferrite once the pearlite is consumed.

New grains of austenite nucleate at pearlite colony boundaries. As the diffusion distances for carbon from the dissolving cementite to the ferrite/austenite interface are small (smaller or equal to half the

spacing characteristic of the pearlite), these grains grow extremely fast, to the extent that pearlite is sometimes assumed to transform instantly into austenite, followed by the advance of the interface into the ferrite.

When austenite starts to grow into ferrite, carbon has to partition to the austenite/ferrite interface for the reaction to proceed, so the diffusion rate of carbon in austenite becomes one of the limiting factors, but the distances involved in this diffusion process are much larger, and the rate of transformation will depend on the morphology, distribution and volume fractions of the phases present.

Any model aiming to describe the austenitisation of a hypoeutectoid steel has to deal with all the parameters referred to above. Austenitisation must clearly be microstructure sensitive. Thermodynamic equilibrium limits the extent of transformation at long times, while nucleation of austenite in pearlite colonies and diffusive processes are expected to control the rates of transformation.

Microstructure characterisation is based on the banded microstructure presented by rolled steels (Fig.2), where $2l_\alpha$ and $2l_P$ are respectivelly, the thicknesses of the bands formed by ferrite grains and pearlite colonies. A characteristic dimension of a pearlite colony is defined as l_{col}, and the pearlite interlamellar spacing as $2l_e$ (Fig.3). In the case of an alloy where the microstructure is not so severely banded, these parameters can still represent the extent of each phase in a way which accounts for austenite formation.

Austenite nucleates at the surfaces of the pearlite colonies. An approach based on classical nucleation theory (Ref.4) is used to calculate the dependence of nucleation rate on temperature. The nucleation rate per unit time in a single colony I is calculated using Equation [6], where N_0 is the

number of nucleation sites per unit volume, and C_0 is a fitting parameter. As the active nucleation sites are all assumed to be located at the surface of the pearlite colonies, and not evenly distributed in the volume of material the ratio between colony surface to volume has to be determined. This factor takes into account the coarseness of the pearlitic microstructure. This calculation gives the factor $6/l_{col}$. k is the Boltzmann constant; R the gas constant; h the Planck constant; Q is an activation energy representing the barrier for the iron atoms to cross the interface, estimated to be 270,000 J mol^{-1} (Ref.5). T is the absolute temperature and G^* is the activation free energy for nucleation.

The activation free energy for nucleation is determined from a balance of interface and volume energies of the critical nucleus, which is assumed to be spherical. The austenite/ferrite interface energy at nucleation is considered to be σ=0.025 J m^{-2} (Ref.5). The change of free energy from a cementite and ferrite mixture to austenite has been determined in this work using a thermodynamic package software, MTDATA.

Once the new grains of austenite have nucleated, their rate of growth, up to the equilibrium volume fraction, has been assumed to be determined by the diffusion of carbon in austenite, from the decomposing cementite, to the boundary between ferrite and austenite. The velocity of that interface can be determined from a mass balance of carbon and the diffusion equation, arriving to equation [7], where v^{int} is the velocity of the interface at a given distance r from the ferrite/cementite interface, D is the diffusion of carbon in austenite as a function of carbon content of the alloy and temperature, $c_{\gamma\alpha}$ and $c_{\alpha\gamma}$ are the carbon content of austenite and ferrite in paraequilibrium with each other, and $c_{\gamma\theta}$ is the carbon composition of austenite in paraequilibrium with cementite, determined following (Ref.6). The advancement direction of the interface is perpendicular to the diffusion of carbon and a function of the diffusion distance r. That obviously means that the advancing front of austenite will show different velocities from the α/θ interface to the centre of the ferrite lamina

(Fig.4). As the velocity of the interface is a function of the inverse of the diffusion distance, the interface would not be flat, but present instead a double hyperbolic contour. In order to avoid increasing the complexity of the model with capillarity effects, an average advance velocity for a flat interface is used (equation [8]). Since many austenite nuclei may start to grow, impingement must is taken into account using Avrami's extended volume method (Ref.7-9).

Once all the pearlite has been transformed to austenite, the α/γ interface keeps advancing into the ferrite grains until all the material has been austenitised. This interface is considered to be flat. As the diffusion distances become larger, the velocity of the interface becomes smaller. Ferrite grains are assumed to be flat plates, with an average thickness of $2l_\alpha$ so that there is no need to consider impingement between growing particles.

Quench:

To model the decomposition of austenite, a model based on the work of many previous studies has been compiled. The cooling curve supplied by the temperature evolution submodel is split into two constant cooling rates, which govern the progress of reconstructive and displacive transformations respectivelly. Simultaneous precipitation reactions can be dealt with using the method for simultaneous reactions developed by Robson and Bhadeshia (Ref.10), extending classic kinetics theory (Ref.4). Jones and Bhadeshia (Ref.11) have adapted such method to deal with simultaneous reconstructive reactions of the decomposition of austenite into allotromorphic ferrite, pearlite, and Widmanstätten ferrite.

The displacive transformation to bainite is modeled following Takahashi and Bhadeshia (Ref.12), whose method is based in the determination of several continuous cooling curves for the formation of different increasing volume fractions of bainite, by the determination of the incubation period for the onset of transformation in each case. Transformation to martensite and the determination of the

volume fraction of retained austenite is calculated using the Koistinen and Marburger equation (Ref.13).

Application of the models:

The accuracy of the heat evolution model has been tested by comparison with experimental data of the evolution of temperature during induction hardening. The experimental test has been performed using the same technology used to induction harden components for constant velocity joints for automobiles. The only difference with the real manufacturing conditions was that the component was manufactured in Inconel, to avoid phase transformation. To measure the temperature evolution during the test, several holes were drilled in the sides of the component and thermocouples fitted at 1 mm of depth from the outer surface (Fig.5). The numeric model needs several input parameters, some of which are not easily measured (dead time, input heat flux, water sprays heat transfer coefficient), and have been deduced from experimental data as fitting parameters. The characteristics of the alloy and other inputs of the model are described in Table 1.

Density	$8.5 \cdot 10^3$ kg m^3	Induction heat flux	$1.9 \cdot 10^8$ W m-2
Specific heat	460 J kg^{-1} K^{-1}	Air heat transfer	6 W m^{-2} K^{-1}
Resistivity	$9.8 \cdot 10^{-7}$ Ohm	Water sprays heat transfer	$22 \cdot 10^3$ W m^{-2} K^{-1}
Conductivity	15.5 W K^{-1} m^{-1}	Dead time	0.25 s

Table 1: Input parameters used by the model. The thermal properties of Inconel are refered to 20°C.

The accuracy of the predictions is remarkable (Fig.6), especially above 300ºC, where most of the studied phenomena occur. The small discrepancies between measured and calculated values are easily explained. During heating the heat flux induced into the metal has been considered constant. However, this is a parameter that will certainly change as a function of temperature. The yield of the installation will also increase with time until it reaches a steady state value, instead of starting to function at that value, as assumed in the calculations. During cooling, a similar simplification has been used, allowing the heat transfer coefficient of the water spraying system to remain constant

throughout the cooling process. This assumption still gives good predictions at high temperatures, but clearly does not hold when the temperature of the component approaches room temperature.

To test the predictions of the austenitisation model, a standard set of experiments has been designed. This set of experiments can then be used to compare the capability of the model to predict the effects of other parameters like composition and microstructure. Six experiments have been used, consisting of heating a steel sample into the intercritical range for a short to medium time (Fig.7), so that a partial transformation to austenite is expected, and using suitable time and temperature conditions so that the full range of partial transformation is covered, from barely no transformation to almost complete reaction. Experimental data were collected using a thermomechanical simulator (Thermecmastor-Z), using hollow samples to minimise their thermal mass. The samples were swiftly heated to a temperature below A_{c1}, and then brought into the intercritical temperature range for a short period of time, to achieve various degrees of partial transformation to austenite, and finally quenched with helium jets. Due to the fast heating and cooling rates planned, at the limits of the equipment used, some of the samples did not follow precisely the planned thermal cycle. The real thermal history was recorded during the experiments and that information, together with composition and microstructural description of the samples, was fed into the model and its results compared with experimental data. The model was tested using the standard set of experiments against two steels of different composition, and slightly different microstructure. As shown in (Fig.8) and (Fig.9), the predictions of the model give an excellent description of the experiments.

To illustrate the use of the quenching module of the model, and ensure that it is able to predict the correct metallurgical trends, a continuous cooling transformation (CCT) diagram has been calculated for a typical alloy used for induction hardening. The alloy considered contains, in wt.%, 0.55 C, 0.22 Si, 0.77 Mn, 0.20 Cr, 0.15 Ni, 0.05 Mo and 0.001 V; and has a grain size of 10 μm.

The following constant cooling rates were used in the calculations: 0.01, 0.1, 1, 10, 20, and $50^{o}Cs^{-1}$. Constant cooling rates higher than $50^{o}C\ s^{-1}$ were considered but this rate is usually enough to obtain martensite structure in the type of alloy studied here. The CCT diagram is shown in (Fig.10).

According to the calculations, at slow cooling rates, ferrite starts forming at a higher temperature than pearlite, but only at the slowest rates does it reach any appreciable amount (1%) before pearlite does. Pearlite forms rapidly, transforming 50% of the austenite shortly after the start of reaction. At a constant cooling rate of $50^{o}C\ s^{-1}$, only 1% of pearlite is formed, transforming most of the austenite to martensite.

Although the complete model still has to be tested, the predictions of the various submodels offer a satisfactory level of acuracy and prove that the overall model will behave in the same way.

Conclusions:

A model to calculate the evolution of the microstructure of a hypoeutectoid steel during induction hardening has been presented. The model has a modular structure, being subdivides in three modules designed to calculate the temperature evolution, austenitisation and decomposition of austenite respectively. These submodels have been proven to be able to predict accurately the temperature evolution and phase transformation behaviour during induction hardening.

Acknowledgements:

The author is grateful to GKNT Ltd. for financial support of this project and to Professor H. K. D. H. Bhadeshia for his supervision and assistance in many phases of this project. Gratitude is expressed as well to Professor D. J. Fray for the provision of laboratory facilities. Special gratitude is expressed to the organisers of the International Conference "Mathematical Modelling and Information Technologies in Welding and Related Processes" for granting the author the opportunity to present this work.

References:

1. *Grum, J.* Induction hardening // In *Handbook of residual stresses and deformation of steel.* ASM International. - 2002.- P. 220-247.
2. *Gaude-Fugarolas, D.* Modelling of transformations during induction hardening and tempering (Ph.D. Thesis) // University of Cambridge.- 2002
3. *Crank, J. and Nicholson, P.* A practical method for numerical evaluation of solutions of partial differential equations of the heat-conduction type // Proceedings of the Cambridge Philosophical Society.- 1947.-N 43.-P.50-67.
4. *Christian, J. W.* Theory of transformations in metals and alloys, Part I // Pergamon Press. Oxford.- 1975
5. *Jones, S. J. and Bhadeshia, H. K. D. H*. Competitive formation of inter- and intra-granularly nucleated ferrite. // Metallurgical and Materials Transactions A.-1997.- N 28A.- P 2005-2013
6. *Akbay, T., Reed, R. C. and Atkinson, C.* Modelling reaustenitisation from ferrite/cementite mixtures in Fe-C steels. // Acta Metallurgica et Materialia.- 1994.- N 47.- P 1469-1480
7. *Avrami, M.* Kinetics of phase change. I // Journal of Chemical Physics.-1939.- N 7.- P 1103-1112
8. *Avrami, M.* Kinetics of phase change. II // Journal of Chemical Physics.- 1940.- N 8.- P 212-224
9. *Avrami, M.* Kinetics of phase change. III // Journal of Chemical Physics.- 1941.- N 9.- P 177-184
10. *Robson, J. D. and Bhadeshia, H. K. D. H*. Modelling precipitation sequences in power plant steels. Part 1 -Kinetic theory // Materials Science and Technology.-1997.- N 13.- P 631-639
11. *Jones, S. J. and Bhadeshia, H. K. D. H*. Kinetics of the simultaneous decomposition of austenite into several transformation products. // Acta Materialia.-1997.- N 28A.- P 2005-2013
12. *Takahashi, M. and Bhadeshia, H. K. D. H.* A model for the microstructure of some advanced bainitic steels // Materials Transactions, JIM.-1991.- N 32 (8).- P 689-966
13. *Koistinen, D. P. and Marburger, R. E*. A general equation prescribing the extent of the austenite-martensite transformation in pure iron-carbon alloys and plain carbon steels. // Acta Metallurgica.- N 7.- P 59-60

$$\alpha \frac{\partial^2 u}{\partial x^2} = \frac{\partial u}{\partial t} \tag{1}$$

$$u(x,0) = 0 \tag{2}$$

$$\frac{\partial u}{\partial x}\Big|_{x=0} = 0 \tag{3}$$

$$\frac{\partial u}{\partial x}\Big|_{x=1} = \frac{\dot{q}}{k} \tag{4}$$

$$\frac{\partial u}{\partial x}\Big|_{x=1} = -\frac{h}{k} u(1,t) \tag{5}$$

$$I = C_0 \, N_0 \, \frac{6}{l_{col}} \, \frac{kT}{h} \exp\left(-\frac{G^* + Q}{RT}\right) \tag{6}$$

$$v^{int} \approx \frac{D}{r} \left(\frac{c'^{\beta} - c'^{\alpha}}{c'^{\alpha} - c^{ref}} \right) \tag{7}$$

$$\bar{v}^{int} = \frac{1}{r_f - r_0} \int_{r_0}^{r_f} \frac{1}{r} D \left(\frac{c'^{\beta} - c'^{\alpha}}{c'^{\alpha} - c^{ref}} \right) dr \tag{8}$$

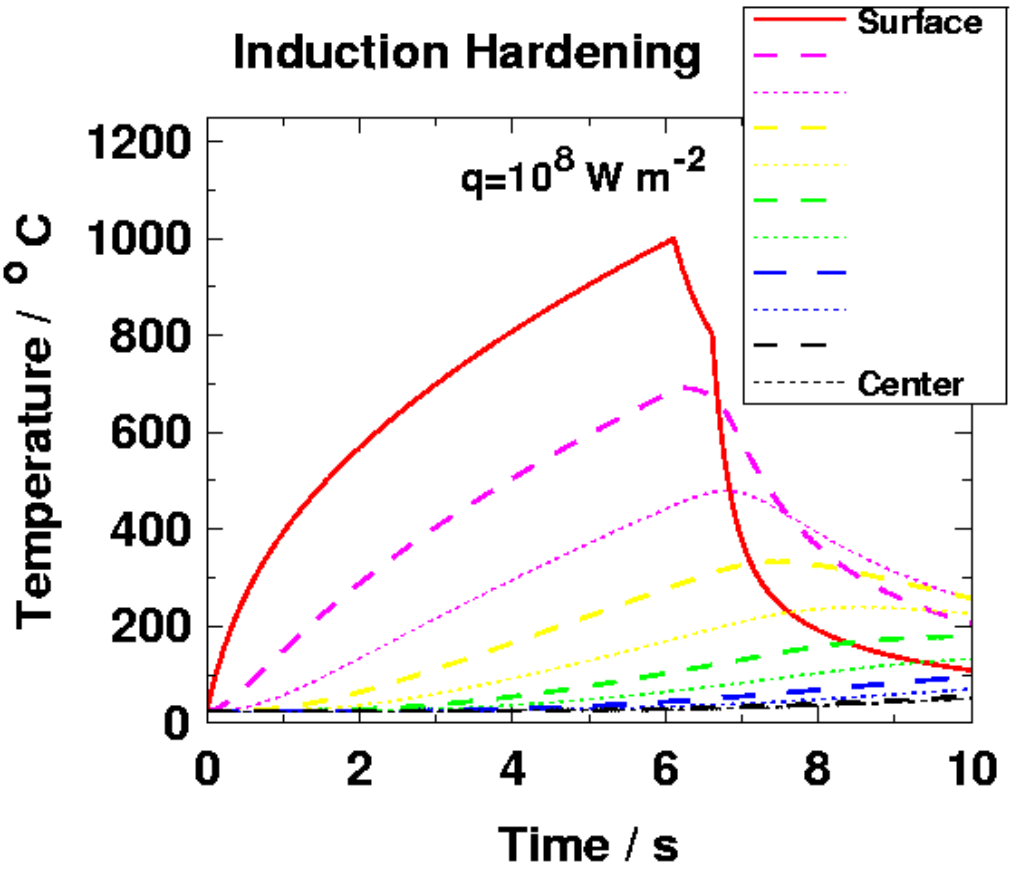

Fig.1. Example plot of the evolution of temperature at different depths in a thick plate of during induction heating as calculated using the finite difference model. q is the heat flux at the surface during the heating stage of the process.

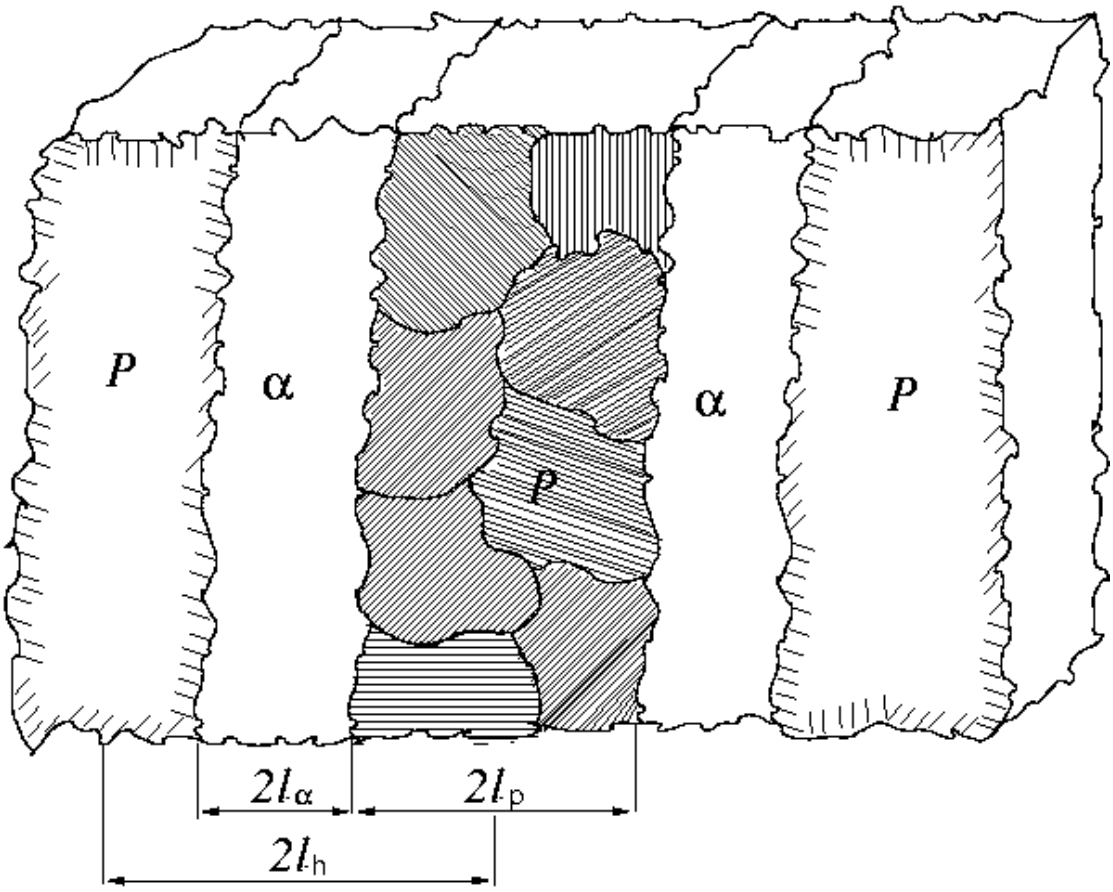

Fig.2 Definition of microstructure parameters *lp*, *lα*, and their sum, *lh*, in a heavily banded microstructure. *P* denotes pearlite and *α* ferrite. These parameters are defined in such a way that they can still be used in other cases where microstructure does not show such level of directionality.

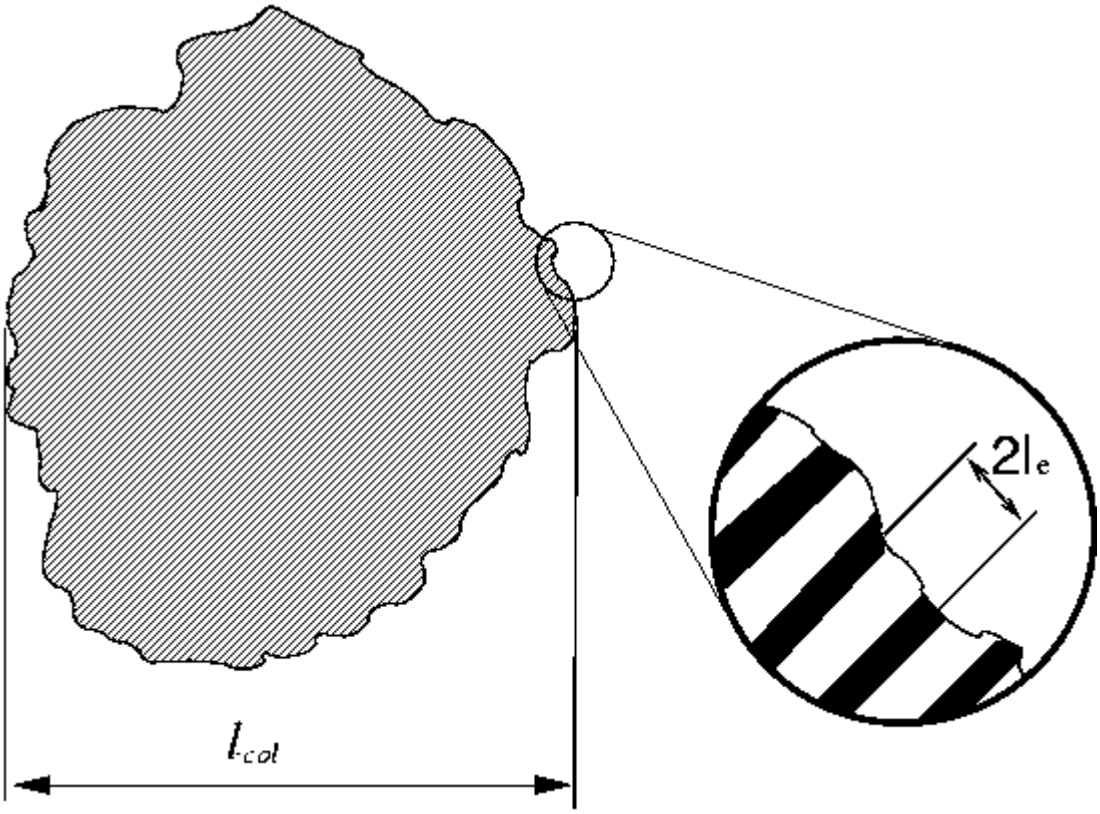

Fig.3 Definition of microstructural parameters l_{col} and l_e. The later characterises the distance between the midthickness of adjacent ferrite and cementite laminae. l_{col} is meant to be a representative dimension of the average pearlite colony.

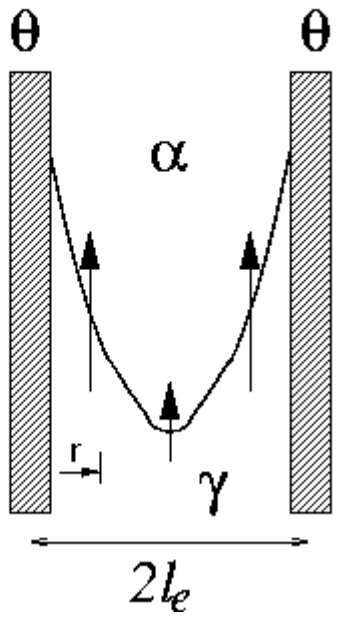

Fig.4 Diffusion distances *r* from cementite to the ferrite/austenite interface vary across the length l_e in the pearlite colony, producing a curved inteface. This profile has been integrated and an averaged advance velocity for the equivalent flat interface has been considered instead.

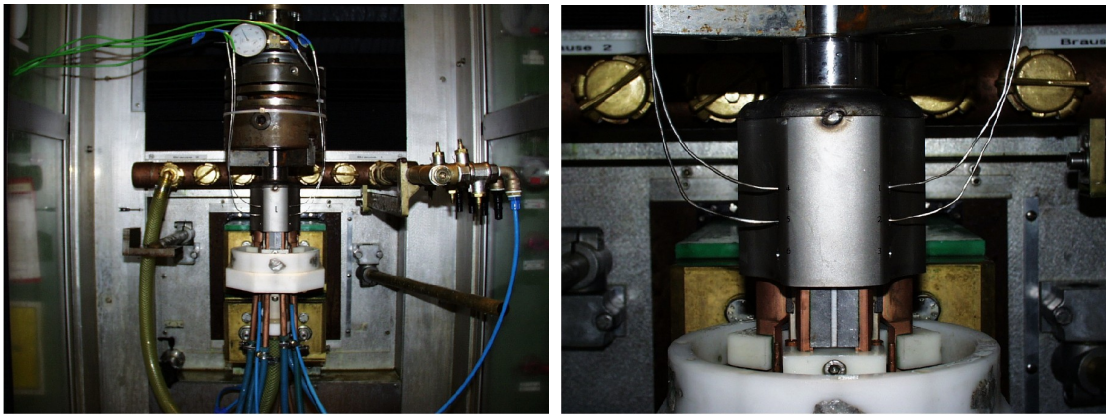

Fig.5 Experimental arrangement for temperature measurement during induction hardening.

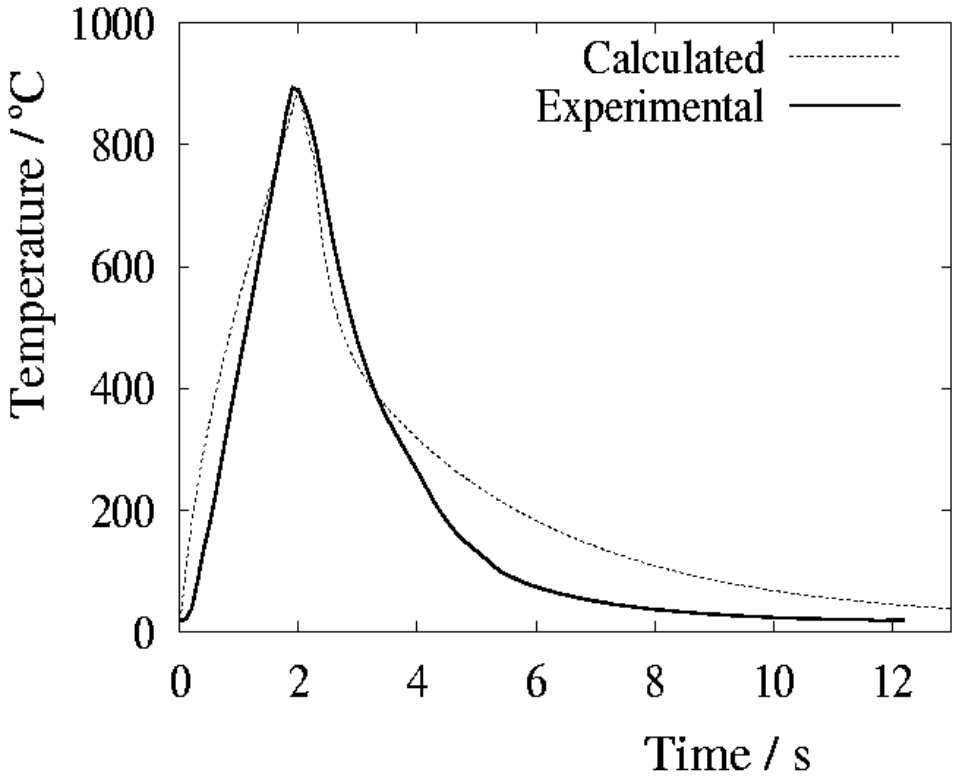

Fig.6 Comparison of the measured thermal evolution and the predicted one for a point 1 mm below the surface of the component.

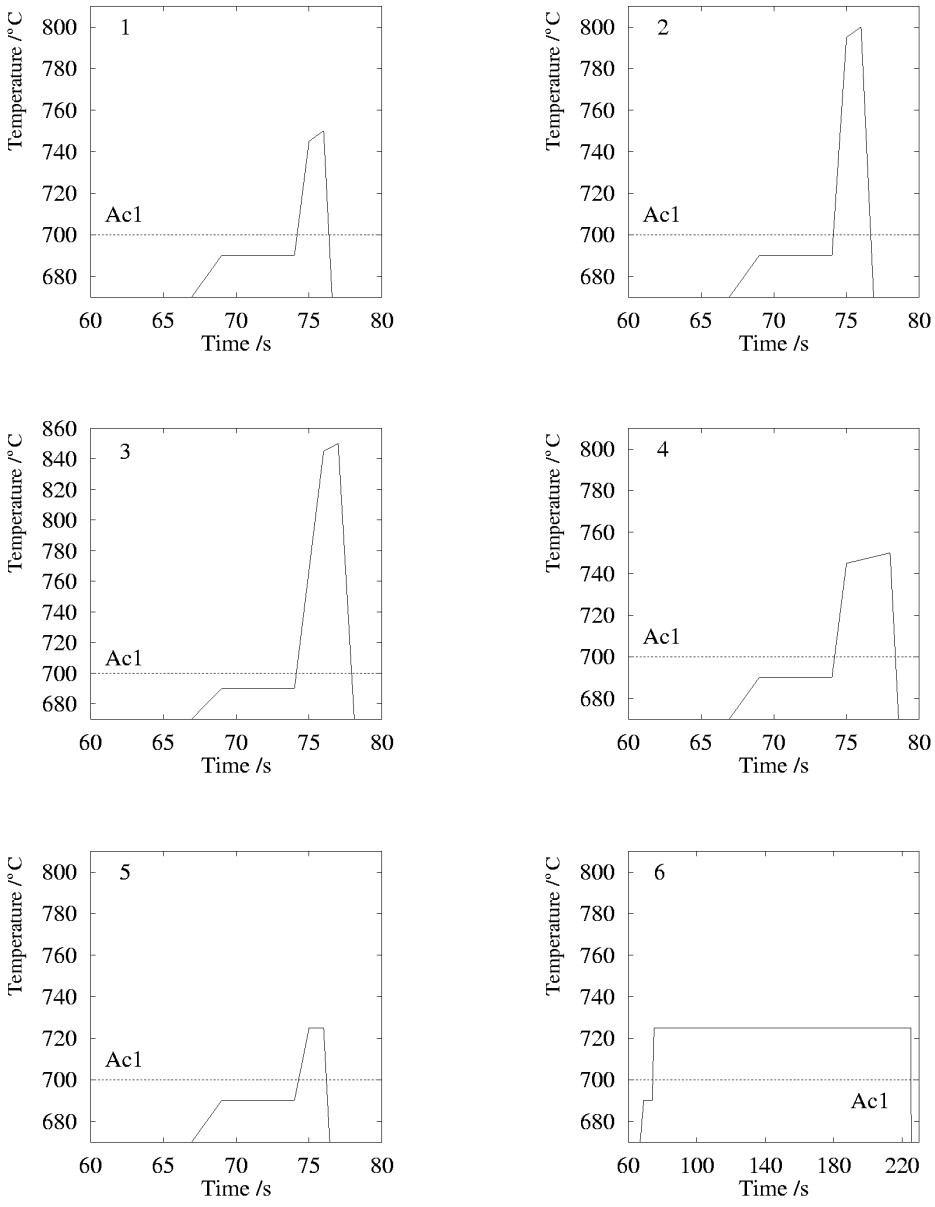

Fig.7 Standard experiments used: dilatometric samples were swiftly heated to a temperature below A_{c1}, and then brought into the intercritical temperature range fpr a short period of time, at a heating rate of 50°C s^{-1}, to achieve various degrees of partial transformation to austenite, and finally quenched with helium jets. Experiments 1, 2, 3 and 5 consider the effect of a short time above A_{c1} reaching different temperatures; experiment 4 considers the effect of an intermediate interval at an intermediate temperature, and finally experiment 6 maintains the sample at a low austenitisation temperature for a long time with the aim of reaching the equilibrium volume fraction of transformation.

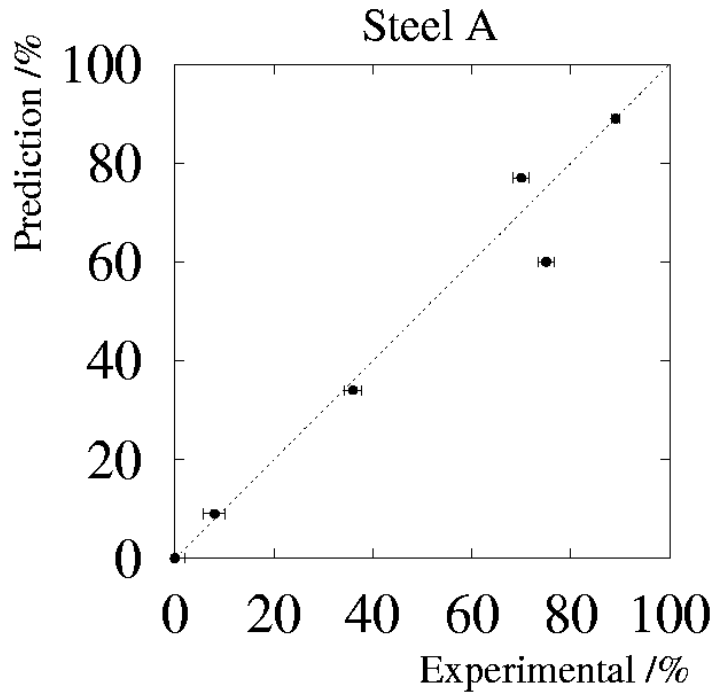

Fig.8 Predictions of volume fraction of austenite against experimental results for one of the alloys considered, denominated Steel A. Numbers refer to experiment number. Error bars correspond to 1 standard deviation in the measurement of the volume fraction.

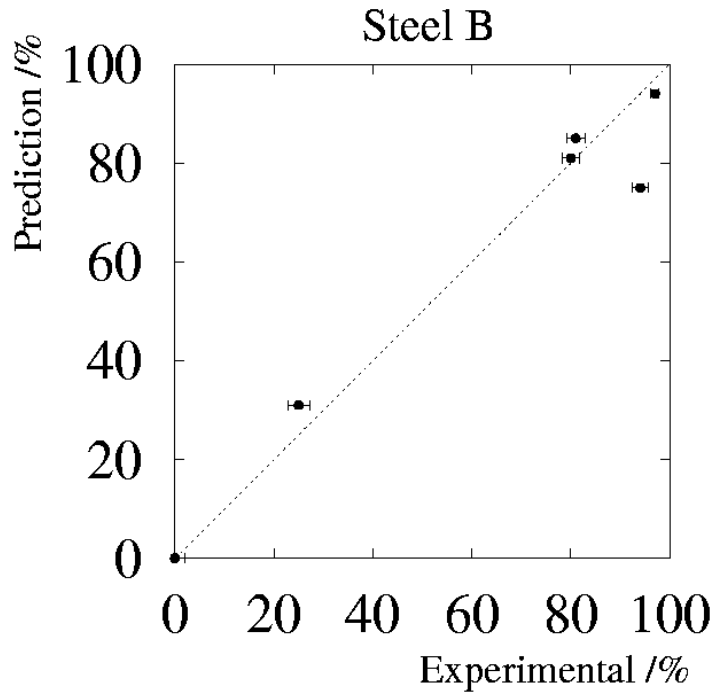

Fig.9 Predictions of volume fraction of austenite against experimental results for one of the alloys considered, denominated Steel B. Numbers refer to experiment number. Error bars correspond to 1 standard deviation in the measurement of the volume fraction.

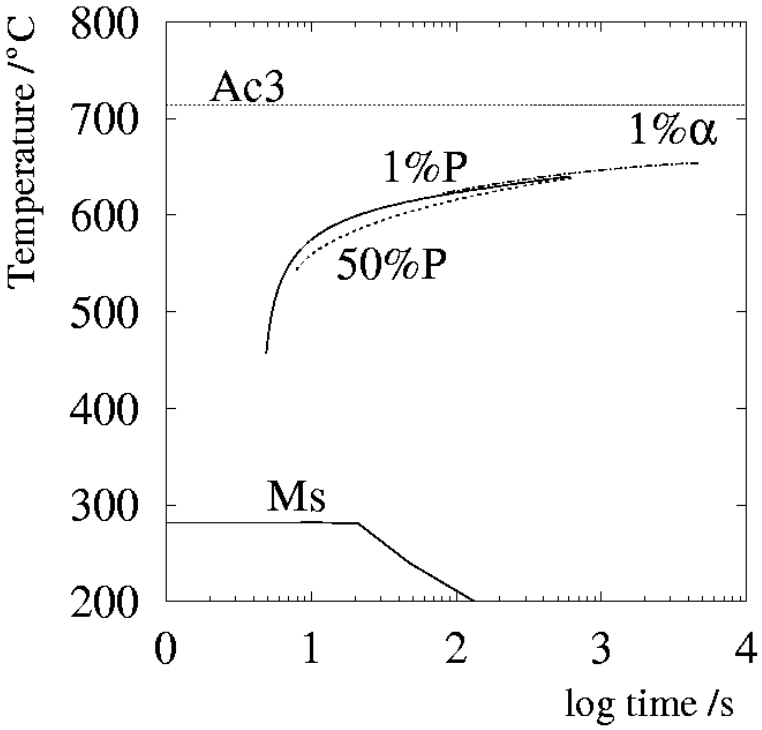

Fig.10 Constant cooling transformation diagram for induction hardening steel, considering a grain size of 10 μm. α stands for ferrite, P for pearlite, A_{c3} is the upper critical temperature for transformation to austenite, and M_s is the martensite-start temperature.